The design and characterization of wideband spline-profiled feedhorns for Advanced ACTPol

Simon, Sara, Austermann, Jason, Beall, James, Choi, Steve, Coughlin, Kevin, et al.

Sara M. Simon, Jason Austermann, James A. Beall, Steve K Choi, Kevin P. Coughlin, Shannon M. Duff, Patricio A. Gallardo, Shawn W. Henderson, Felicity B. Hills, Shuay-Pwu Patty Ho, Johannes Hubmayr, Alec Josaitis, Brian J. Koopman, Jeff J. McMahon, Federico Nati, Laura Newburgh, Michael D. Niemack, Maria Salatino, Alessandro Schillaci, Benjamin L. Schmitt, Suzanne T. Staggs, Eve M. Vavagiakis, Jonathan Ward, Edward J. Wollack, "The design and characterization of wideband spline-profiled feedhorns for Advanced ACTPol," Proc. SPIE 9914, Millimeter, Submillimeter, and Far-Infrared Detectors and Instrumentation for Astronomy VIII, 991416 (19 July 2016); doi: 10.1117/12.2233603

SPIE.

Event: SPIE Astronomical Telescopes + Instrumentation, 2016, Edinburgh, United Kingdom

The design and characterization of wideband spline-profiled feedhorns for Advanced ACTPol

Sara M. Simon[a], Jason Austermann[b], James A. Beall[b], Steve K. Choi[a], Kevin P. Coughlin[c], Shannon M. Duff[b], Patricio A. Gallardo[d], Shawn W. Henderson[d], Felicity B. Hills[c], Shuay-Pwu Patty Ho [a], Johannes Hubmayr[b], Alec Josaitis[c], Brian J. Koopman[d], Jeff J. McMahon[c], Federico Nati[e], Laura Newburgh[f], Michael D. Niemack[d], Maria Salatino[a], Alessandro Schillaci[g], Benjamin L. Schmitt[e], Suzanne T. Staggs[a], Eve M. Vavagiakis[d], Jonathan Ward[e], and Edward J. Wollack[h]

[a]Department of Physics, Princeton University, Princeton, NJ 08544, USA
[b]National Institute of Standards and Technology, 325 Broadway Mailcode 817.03, Boulder, CO 80305, USA
[c]Department of Physics, University of Michigan, Ann Arbor, MI 48109, USA
[d]Department of Physics, Cornell University, Ithaca, NY 14853, USA
[e]Department of Physics and Astronomy, University of Pennsylvania, Philadelphia, PA 19104, USA
[f]The Dunlap Institute, University of Toronto, Toronto, Ontario, Canada M5S 3H4
[g]Institute of Astrophysics, Pontificia Universidad Católica de Chile, Toronto, Santiago, Chile
[h]NASA Goddard Space Flight Center, Greenbelt, MD 20771, USA

ABSTRACT

Advanced ACTPol (AdvACT) is an upgraded camera for the Atacama Cosmology Telescope (ACT) that will measure the cosmic microwave background in temperature and polarization over a wide range of angular scales and five frequency bands from 28-230 GHz. AdvACT will employ four arrays of feedhorn-coupled, polarization-sensitive multichroic detectors. To accommodate the higher pixel packing densities necessary to achieve AdvACT's sensitivity goals, we have developed and optimized wideband spline-profiled feedhorns for the AdvACT multichroic arrays that maximize coupling efficiency while carefully controlling polarization systematics. We present the design, fabrication, and testing of wideband spline-profiled feedhorns for the multichroic arrays of AdvACT.

Keywords: Advanced ACTPol, feedhorn, spline-profiled, wideband, polarization, cosmic microwave background

1. INTRODUCTION

The polarization of the cosmic microwave background (CMB) can be decomposed into even (E-mode) and odd (B-mode) parity components.[1,2] If a period of inflation occurred in the early universe, the gravitational waves produced could leave a measurable imprint in the B-mode spectrum of the CMB at large angular scales (for a recent review, see Abazajian et al.[3]). The E-mode signal is dominated by scalar density perturbations but would also have a component from inflationary gravitational waves. Measuring the amplitude of the B-mode signal could give the energy scale of inflation and is quantified by the tensor-to-scalar ratio r. AdvACT will replace the ACT Polarimeter (ACTPol), which is currently conducting observations.[4,5] AdvACT's high resolution and planned use of continuously-rotating half-wave plates (HWPs) will enable it to make sensitive measurements of CMB polarization at both small and large angular scales. These data will allow improved constraints on the

Further author information: (Send correspondence to S.M.S.)
S.M.S.: E-mail: smstwo@princeton.edu

Millimeter, Submillimeter, and Far-Infrared Detectors and Instrumentation for Astronomy VIII, edited by Wayne S. Holland, Jonas Zmuidzinas, Proc. of SPIE Vol. 9914, 991416
 · doi: 10.1117/12.2233603

fundamental physics of the universe, including the sum of the neutrino masses and the amplitude of inflationary B-modes. AdvACT will sequentially field four feedhorn-coupled arrays of multichroic polarization-coupled detectors in the three optics tubes. A high frequency (HF) array with 150/230 GHz coverage will be fielded first and then supplemented with two mid-frequency (MF) arrays with 90/150 GHz sensitivity. Next, one MF array will be replaced with a low frequency (LF) array that has 28/41 GHz coverage.[6]

AdvACT will use the available focal plane area more efficiently with multichroic pixels fabricated on a single 150 mm wafer for each array. The use of 150 mm wafers enables a higher detector packing density than tiling 3 inch wafers as in ACTPol, leading to a higher sensitivity, which is only achievable through the development of feedhorns that have a small aperture while maintaining high beam coupling efficiency. Asymmetry between the E-plane and H-plane beams can lead to temperature to polarization leakage and E-mode to B-mode leakage. An ideal horn for AdvACT would have high beam coupling efficiency and maximal symmetry between the E-plane and H-plane beams across the multichroic frequency bands. These features are more easily achieved with larger apertures, so a compromise is required.

Corrugated feedhorns can approach near ideal beam symmetry and are currently used by ACTPol for both of the 150 GHz arrays and the 90/150 GHz array.[7,8] However, for the small aperture sizes desired for AdvACT, the corrugations used in the ACTPol feedhorns represent a non-negligable fraction of the area required by each feed, which decreases the achievable coupling efficiency as defined below in Equation 2. The ring-loaded corrugated horns of ACTPol's 90/150 GHz array (Figure 1) are 7 mm in diameter, but the target pixel spacing for the AdvACT 90/150 GHz array is 5.3 mm. Unlike corrugated feedhorns, small-aperture conical feedhorns (Figure 2) have near maximal beam coupling efficiency but poor beam symmetry. Spline-profiled feedhorns (Figure 2) can be designed to interpolate between these cases and optimize a combination of beam symmetry and beam coupling efficiency.[9] In Section 2, we present the AdvACT spline-profiled feedhorn design process followed by the fabrication process in Section 3, the electromagnetic modeling of the AdvACT feedhorns in Section 4, and measurements of the first fabricated AdvACT feedhorn array in Section 5.

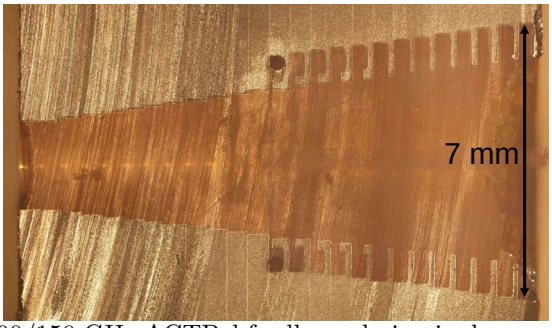

Figure 1: A cross section of the 90/150 GHz ACTPol feedhorn design is shown above. The first five corrugations on the left are ring-loaded. The dark spots in the bottom ring-loaded features are air bubbles in the wax filling the feedhorn, not defects. The pixel-to-pixel spacing on the AdvACT 90/150 GHz arrays is too small to allow for the corrugated feedhorn design.

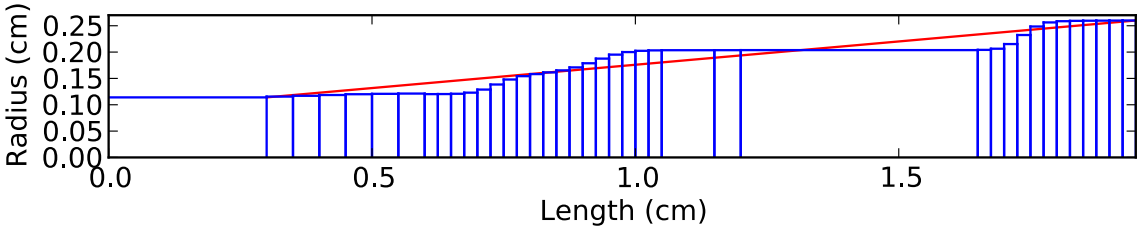

Figure 2: The final optimized 90/150 GHz spline-profiled feedhorn design is shown above in blue with its full waveguide section. The 90/150 GHz conical feedhorn design that was used as a comparison to the spline-profiled horn is shown in red. The conical design is the same length as the spline-profiled feedhorn without its waveguide section and has the same input and output aperture sizes.

2. FEEDHORN DEVELOPMENT

The wideband spline-profiled feedhorns for AdvACT are designed by numerical optimization. We use a Markov chain Monte Carlo (MCMC) algorithm to optimize a feedhorn profile by minimizing a penalty function p over a set of linearly spaced frequencies across the desired observation band. The penalty function is defined as

$$p \equiv \sum_{\text{Frequency}} \sum_{\theta=0}^{\theta=\theta_{stop}} (E^2 - H^2)^2, \tag{1}$$

where E and H are the amplitudes of the E-plane and H-plane beams (respectively), θ is the radial coordinate of the beam in degrees, and $\theta_{stop} = 20.4^\circ$ is defined by the 1 K Lyot stop of the AdvACT optics.[10] The beam coupling efficiency is defined as

$$\text{Beam Coupling Efficiency} = \frac{\int_0^{\theta_{stop}} \frac{1}{2}(E^2 + H^2) \sin\theta \, d\theta}{\int_0^{180^\circ} \frac{1}{2}(E^2 + H^2) \sin\theta \, d\theta}. \tag{2}$$

We do not optimize on the beam coupling efficiency, but it is used as a selection criterion for each feedhorn candidate after the MCMC optimization is complete.

Each MCMC optimization first inputs a given feedhorn profile into an electromagnetic simulator to determine the E-plane and H-plane beams and calculates the penalty function p. The electromagnetic mode-matching routine for azimuthally symmetric circular waveguide sections, CCORHRN*, is used to calculate the radiation pattern for the feedhorn. The thickness of each waveguide section in the simulation is determined by fabrication requirements (see § 3).

Next the optimization produces a new feedhorn profile by randomly varying the basis parameters of the previous feedhorn profile. The feedhorn profiles use a monotonically increasing basis to allow for the possibility of direct machining feedhorns into Al substrates. The input aperture radius of the feedhorn is determined by the desired cutoff frequency of the waveguide section of the horn. In the close-packed regime of AdvACT, the radius of the output aperture is constrained by the pixel-to-pixel spacing on the array. The minimum distance that the fabrication process allows between feedhorn walls is 100 μm, so the diameter of the output aperture is thus 100 μm less than the pixel-to-pixel spacing.

Because the penalty function does not explicitly include consideration of the beam coupling efficiency, we impose additional criteria that each profile must pass before being input to CCORHRN. There is a class of feedhorns that consist of an almost constant waveguide section and a sharp flare at the end of the horn. These profiles lead to highly symmetric beams, but they do not use the full aperture of the horn and thus have extremely poor beam coupling efficiency. Because of their low penalty functions, the MCMC simulations will converge to these solutions if they are not eliminated. If the criteria are failed, the simulation produces another random feedhorn profile. If the criteria are passed, the feedhorn profile is input into the electromagnetic simulator and the optimization process is repeated for a pre-determined number of iterations.

To explore the full range of profiles, the final feedhorn design code creates a large number of random profiles and uses them to seed parallel MCMC optimizations. Each MCMC optimization runs for 10,000 iterations and optimizes on the same ~ 20 frequencies across the observation bands. The code is run on a 40 core computer at the University of Michigan, which allows for 30 parallel optimizations to run at once. By using parallel MCMC optimizations, the run time of the feedhorn optimization has been reduced to less than two days. Several runs are completed for each feedhorn design. The profiles that seed individual MCMC runs can be predefined or are otherwise random profiles. Thus, promising profiles from previous runs can be further optimized by subsequent runs.

After the horn design is finalized, a length of waveguide section is added to the detector side of the feedhorn to sharpen the waveguide cutoff. For the 150/230 GHz and 90/150 GHz feedhorns, higher waveguide cutoff frequencies were desired than the final minimum feedhorn radii provided, so there are small steps in radius to

*YRS Associates, YRS Rahmat-Samii et al. (1995)

the waveguide sections as seen in Figures 2 and 3. Additionally, a photonic choke with a waveguide section equal to that of the feedhorn is added to the detector side of the feedhorn stack to prevent leakage between the feedhorns and the waveguide interface plate (WIP) that couples the feedhorns to the orthomode transducer on the detector wafer. The photonic choke consists of 415 μm wide square pillars with a spacing of 705 μm for the 150/230 GHz feedhorn and 668 μm wide pillars with a 1135 μm pitch for the 90/150 GHz feedhorn.[11] The 150/230 GHz photonic choke wafer has a 400 μm thick flat section on the feedhorn side of the choke and a section with 200 μm tall pillars on the WIP side. For the 90/150 GHz horns, the pillar height is 100 μm. Figure 4 shows the photonic choke on the fully assembled 150/230 GHz feedhorn array. The 150/230 GHz and 90/150 GHz feedhorn designs have been finalized and are shown in Figures 2 and 3, respectively. The 28/41 GHz feedhorn is still under development.

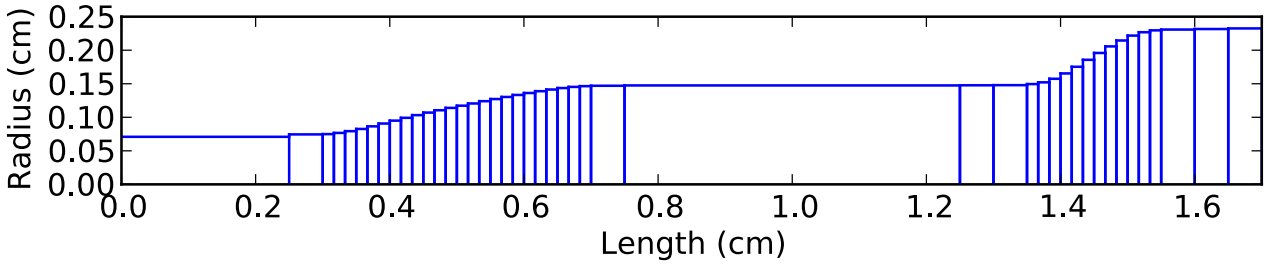

Figure 3: The final 150/230 GHz feedhorn design is shown above, including its waveguide section. The cutoff frequency of the feedhorn defines the low edge of the 150 GHz bandpass. The waveguide section thus serves as a high-pass filter that was designed after the rest of the feedhorn design was optimized. The final feedhorn includes a step down in radius between the feedhorn and waveguide sections to provide a higher cutoff frequency.

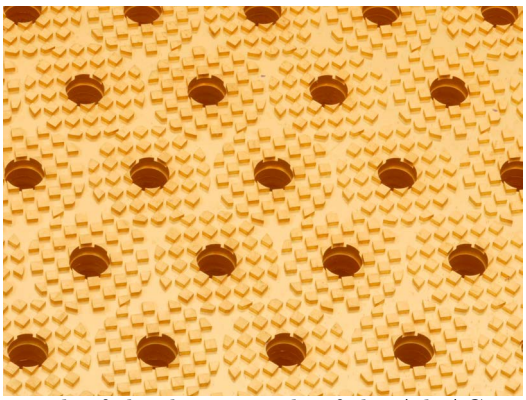

Figure 4: Shown above is a photograph of the detector side of the AdvACT 150/230 GHz feedhorn array. The photonic choke prevents leakage between the interface of the feedhorn stack and the WIP and is the last layer of the feedhorn stack before the WIP.

3. FABRICATION

The monolithic 90/150 GHz and 150/230 GHz AdvACT feedhorn arrays are fabricated at the National Institute of Standards and Technology (NIST) in Boulder.[12] Each array consists of stacked Si wafers that are each etched, coated with a seed layer of 200 nm Ti and 1 μm of Cu, aligned, glued on the edges with Stycast 2850 FT epoxy[†], and electroplated with 3 μm of Cu followed by 3 μm Au. Using photolithography and deep reactive ion etching (DRIE), each Si wafer has one or two layers of the feedhorn profile etched into it. The 150/230 GHz array uses double-etched custom 333 μm wafers to achieve a 167 μm step size. The 90/150 GHz array has a step size of 250 μm and can thus be fabricated with single etched 250 μm and 500 μm wafers. The 28/41 GHz feedhorn is

[†]Emerson and Cuming. Billerica, MA 01821.

designed with 500 μm sections and will be either direct machined into Al or fabricated out of stacked laser-cut 500 μm Si wafers. Figure 5 shows the fully assembled 150/230 GHz feedhorn array. While the spline-profiled feedhorns are longer than the ring-loaded corrugated feedhorns, they do not require triple-etched wafers like the ring-loaded features and are thus simpler and faster to fabricate.

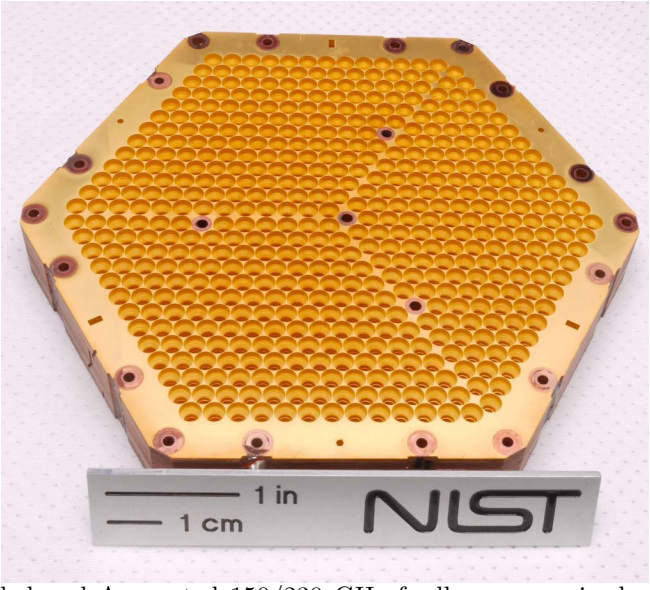

Figure 5: The fully assembled and Au coated 150/230 GHz feedhorn array is shown above. To assemble the array, individual wafers are stacked up, aligned with dowel pins, and glued together.

4. FEEDHORN MODELING

Before fabrication, the feedhorn designs are validated by simulating the beams using both CCORHRN and an electromagnetic finite element method solver called High Frequency Structure Simulator[‡] (HFSS) to simulate their properties and response to fabrication tolerances. We compare the 150/230 GHz and 90/150 GHz feedhorn designs to conical feedhorns with the same length and aperture sizes as the spline-profiled feedhorns. Additionally, we compare the 150/230 GHz design to a scaled version of the 90/150 GHz corrugated feedhorn from ACTPol that fits within the desired pixel-to-pixel spacing. Using the simulated HFSS beams, we calculate the beam coupling efficiency, cross-polarization, far field beams including the instrument Lyot stop, and the polarization leakages in the power spectra assuming a pair-differenced detector pair (an extreme case for AdvACT, which plans to use continuously-rotating HWPs). The 150/230 GHz and 90/150 GHz wideband spline-profiled feedhorns developed for AdvACT have good beam symmetry while retaining a high beam coupling efficiency. Based on this evaluation, the 90/150 GHz spline-profiled feedhorn improves the mapping speed of the array by a factor of $\sim$1.8 over the original ACTPol corrugated design.

4.1 Modeling Fabrication Tolerances

The radial uncertainty achievable by NIST in the etches for each Si wafer in the feedhorn array is $\pm$1-2 μm. To test the radial uncertainty, we scaled all the radii up and down by 2 μm and then individually varied each layer by a random amount from -2 μm to 2 μm. Similarly, the wafer thickness tolerance is $\pm$10 μm, so we scaled all the wafer thicknesses up and down by 10 μm and then randomly varied them to test this tolerance. Additionally, there can be misalignments as the wafers are stacked to make the feedhorn array. The maximum misalignment between wafers is 5 μm with a maximum total misalignment of 10 μm across the entire feedhorn array, which is set by the tolerances in the alignment pin holes. To model this misalignment, we added the maximum displacement

[‡]ANSYS, Inc. Canonsburg, PA 15317

in random directions for the full length of the feedhorn while ensuring that the total misalignment did not exceed 10 μm. All of these tests had a negligible impact on the feedhorn properties described in § 4.2.

Additionally, the DRIE can add a taper as large as 2° to the sidewall of each vertical etch. This effect is typically more pronounced at the edges of the wafer. The DRIE taper minimally decreases the beam symmetry and has a negligible effect at the sub-percent level on the beam coupling efficiency. However, we model the feedhorns both with and without the taper, and, to be conservative, we use the maximal taper of 2° in the calculation of all the quantities described in Sections 4.2 and 4.3.

4.2 Feedhorn Properties

The reflection is modeled in HFSS with the DRIE taper with 1 GHz resolution. Figures 6 and 7 show the reflection of each of the feedhorn candidates for the 90/150 GHz and 150/230 GHz feedhorn designs, respectively. On average, the conical feedhorns have the lowest reflection, but the spline-profiled horns' reflections are better than -20 dB for $\gtrsim$ 90% of their bands.

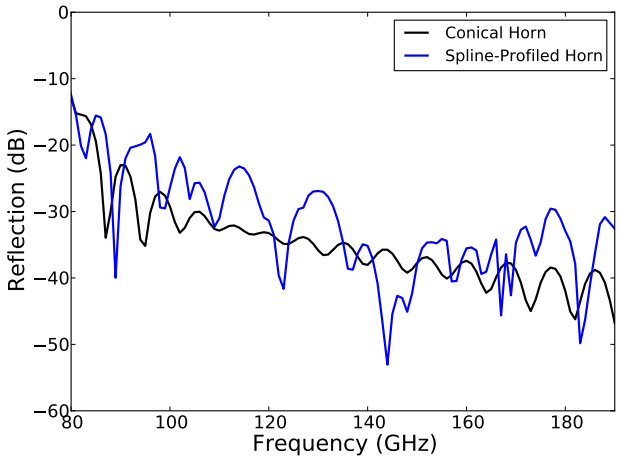

Figure 6: The simulated reflections of each of the conical and spline-profiled feedhorn candidates for the 90/150 GHz feedhorn are shown above. The cutoff frequency of the spline-profiled horn is ∼78 GHz. Simulations were performed with HFSS. Recall that the conical feedhorn design does not have a waveguide section.

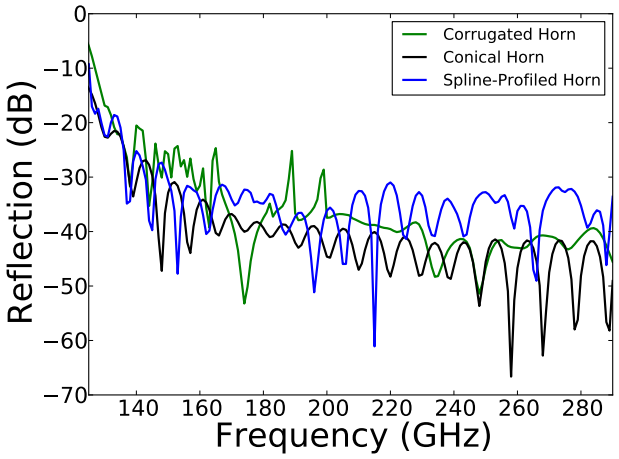

Figure 7: The simulated reflections from HFSS of each of the three 150/230 GHz feedhorn candidates are shown above. The starting frequency of the plot, 125 GHz, is set by the cutoff frequency of the spline-profiled horn, which is ∼124 GHz. Some of the excess reflection at high frequency of the spline-profiled horn is a result of changing the waveguide section of the horn after its full design.

The average cross polarization and beam coupling efficiency in each band for these feedhorn designs is summarized in Table 1. The 90/150 GHz spline-profiled horn has more cross polarization in the low band than the conical horn and less in the high band. For the 150/230 GHz horns, the cross polarization of the spline-profiled horns is less than that of the conical horns. The spline-profiled horn also has less cross polarization in the 150 GHz band than the corrugated horn but slightly more cross polarization in the 230 GHz band. The conical feedhorns have the least beam symmetry, and thus, as expected, their beam coupling efficiency is maximized. For the HF horns, the spline-profiled horn has higher beam coupling efficiency in the 150 GHz band than the corrugated horn but lower beam coupling efficiency in the 230 GHz band.

4.3 Estimation of Polarization Leakage

We estimate the polarization leakages in the power spectra using the simulated co- and cross-polar beams at every 10 GHz across the observation bands from HFSS. The polarization leakages assume a pair-differenced detector pair, which is a strong test of the performance since in AdvACT the HWPs will provide significant mitigation of the systematics and eliminate the need for pair differencing.

Table 1: The cross polarization and beam coupling efficiency of both bands for perfect realizations of the finalized spline-profiled designs as well as the other feedhorn candidates are shown below. The spline-profiled horn model includes the DRIE taper. In the case that there is no DRIE taper, there is a $< 0.5\%$ difference in the beam coupling efficiency, a $< 0.08\%$ difference in the cross polarization of the HF horn, and a $< 0.01\%$ difference in the cross polarization of the MF horn.

Feedhorn	**Band Range (GHz)**	**Cross Polarization**	**Beam Coupling**
MF Spline	80-110	1.7%	46%
MF Spline	125-165	0.3%	69%
MF Conical	80-110	1.1%	49%
MF Conical	125-165	1.3%	77%
HF Spline	125-175	1.0%	66%
HF Spline	195-285	0.4%	77%
HF Conical	125-175	1.3%	72%
HF Conical	195-285	1.6%	90%
HF Corrugated	125-175	1.6%	48%
HF Corrugated	195-285	0.3%	87%

To estimate the far field signal and leakage beams, we calculate the signal and leakage beams using the co- and cross-polar beams from HFSS, mask them so that they go to zero when $\theta > 20.4^\circ$ to account for the Lyot stop, and Fourier transform the masked beams. The far field beams are then normalized by the maximum of the signal beam and averaged across the low and high bands of each feedhorn. We carry out this calculation for pixels sampled across the full extent of the detector array. The central pixel gives the lowest temperature to polarization leakage. While edge pixels exhibit higher leakage, the average leakage beam of pairs of pixels equidistant from the array center on opposite sides of the array approximates the behavior of the central pixel. Therefore, the behavior of the central pixel provides an estimate for the systematics of the array.

We then estimate the window functions[13] of the signal and leakage beams. To account for the rest of the optics, including the 6 m ACT telescope, we normalize the multipole axis by comparing the signal beam window function to a window function of a Gaussian beam with full width at half maximum (FWHM) of $1.3\,n$ arcmin. Here $n = 1$ for the 150 GHz beams to match expectations for CODE V modeling of the telescope and camera optics. We scale n by frequency so that $n = 150/230$ for the 230 GHz beam and $n = 145/90$ for the 90 GHz beam. The measured spectra are then determined by multiplying models of the E-mode and B-mode polarization spectra by the signal window function, the temperature to polarization leakage spectrum (Figures 8 and 9) is determined by multiplying the modeled temperature spectrum by the intensity leakage window function, and the E-mode to B-mode leakage is determined by multiplying the modeled E-mode spectrum by the polarization leakage window function.

The E-mode to B-mode leakage is several orders of magnitude below the B-mode signal. At the percent level, the temperature to polarization leakage is not negligibly small, but MCMC simulations of the 150/230 GHz horn design using the calculated far field beam results at 150 GHz (where the leakage is the worst) determined that the leakage from temperature into the B-modes has a large suppression factor compared to leakage into E-modes, indicating that the temperature to polarization leakage from the feedhorn goes almost entirely into E-modes at a negligible level consistent with the formalism[§] presented in Shimon et al. 2008.[15] Accounting for beam asymmetries in analysis could further mitigate the leakage by an order of magnitude or more, cross-linking in the maps helps identify and quantify this leakage, and the planned HWPs for AdvACT will significantly mitigate the leakage.

[§]The feedhorns presented in this work produce elliptical beams if fed with E_x or E_y polarization. Because the semi-major axes of these beams are orthogonal, the s^2_ψ term vanishes and thus the leakage into B-modes vanishes as shown in Table V of Shimon et al. 2008.

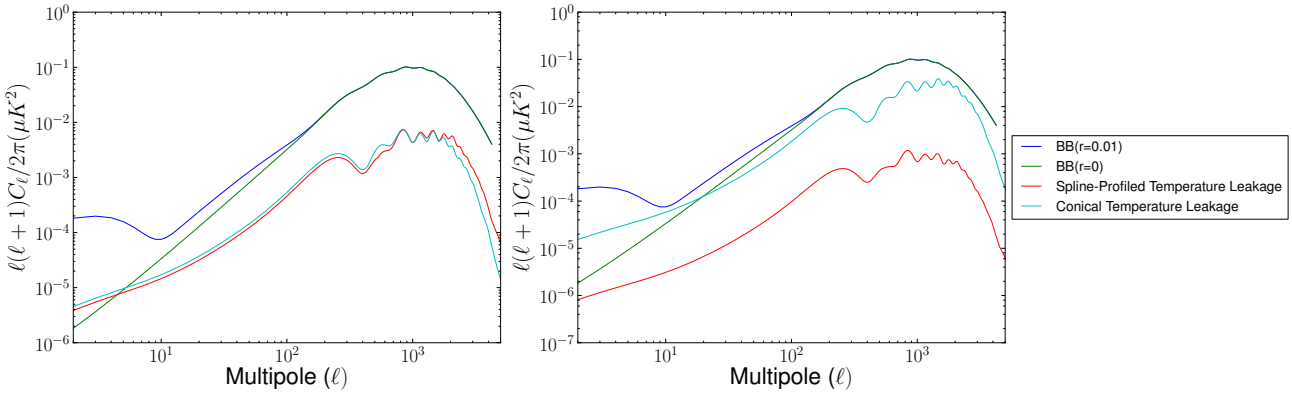

Figure 8: The temperature to polarization leakage of the 90/150 GHz spline-profiled (red) and conical (cyan) feedhorns are plotted with the B-mode signal for $r = 0$ (green) and $r = 0.01$ (blue) for the 90 GHz band (left) and the 150 GHz band (right). The peak in the predicted B-mode spectrum at $\ell \sim 1000$ comes from gravitational lensing of the dominant E-mode signal.[14] The conical feedhorn has slightly more leakage at 90 GHz and significantly more leakage at 150 GHz compared to the spline-profiled feedhorn. It is important to note that this is for the extreme case where the detectors are pair-differenced and no HWP is in use. These leakages can be further mitigated by accounting for beam asymmetries in analysis and by the use of a HWP as planned.

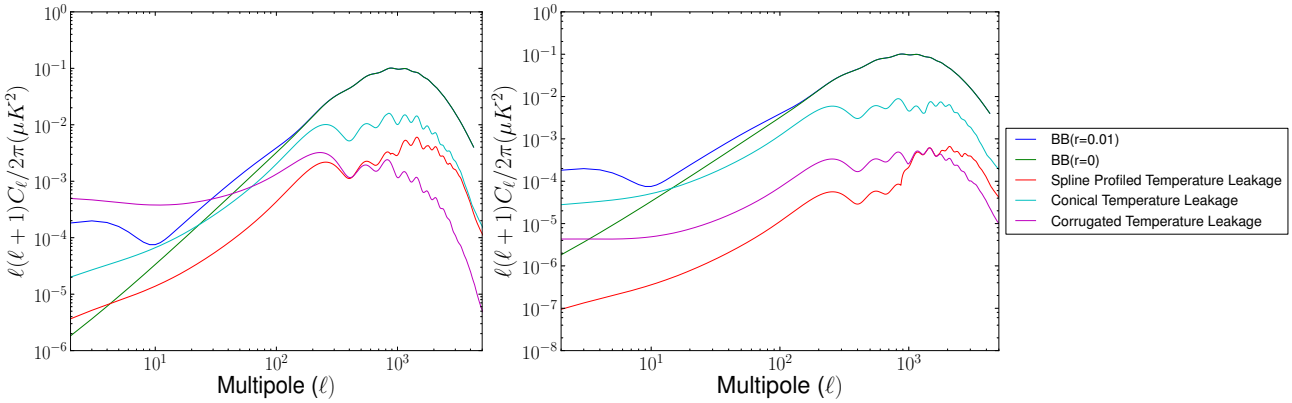

Figure 9: The temperature to polarization leakage of the 150/230 GHz spline-profiled (red), conical (cyan), and corrugated (magenta) feedhorns are plotted with the B-mode signal for $r = 0$ (green) and $r = 0.01$ (blue) for the 150 GHz band (left) and the 230 GHz band (right). On average, the conical feedhorn has the largest total leakage. The leakage from the corrugated horn is higher than that from the spline-profiled horn at large scales and smaller at small scales. The transition to a smaller waveguide section than the horn was optimized for causes a small increase in the leakage at small angular scales in the high band.

5. FEEDHORN MEASUREMENTS

We measured the E-plane, H-plane, and cross-polarization beams of the final 150/230 GHz feedhorn array with 0.5° resolution every 10 GHz across the upper and lower detector bands at four positions across the feedhorn array (as shown in Figure 10) using an ambient-temperature vector network analyzer (VNA) setup at NIST. The NIST VNA beam mapper consists of a transmitter, which sends a signal through the feedhorn being measured and a receiver mounted on a rotating arm as shown in Figure 11. The receiver for the low band (130 GHz-180 GHz) setup uses a conical feedhorn, and the high band setup (200 GHz-270 GHz) uses a diagonal feedhorn that has a square aperture that is rotated 45° with respect to a square waveguide section for the receiver. Because the high frequency band is more sensitive to misalignments and its signal-to-noise is lower than the low band, we repeated the measurements of the high band at a single feedhorn position (position 7) with the transmitter and receiver moved closer together, 1.6° resolution, and AN72 eccosorb foam around the feedhorn array and the receiver to reduce reflections.

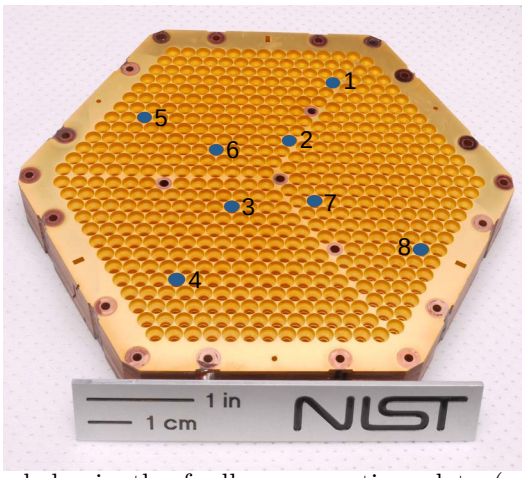

Figure 10: The positions of the holes in the feedhorn mounting plate (not shown) are mapped onto the 150/230 GHz feedhorn array. Positions 1, 2, 7, and 8 were measured.

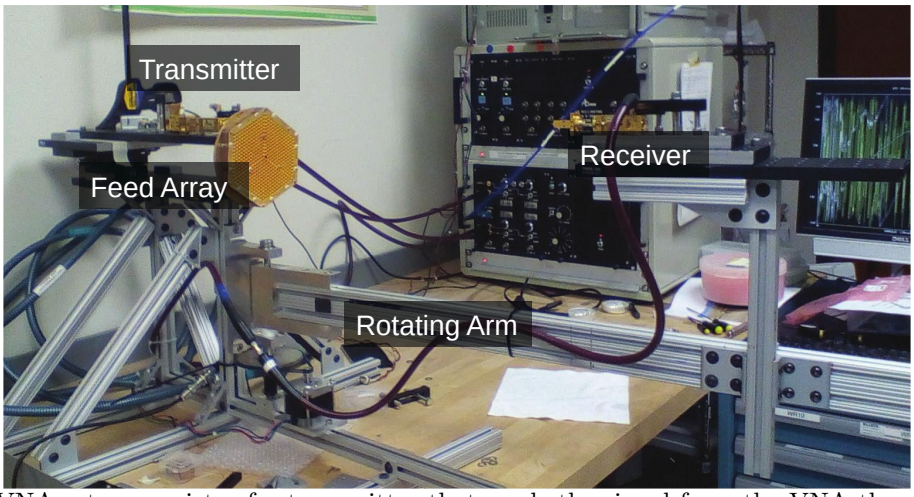

Figure 11: The VNA setup consists of a transmitter that sends the signal from the VNA through the feedhorn array and a receiver on the end of a rotating arm.

The beam measurements are in good agreement with the simulations as shown by Figure 12. The measurements are also consistent among positions on the array as shown by Figure 13, indicating that the feedhorn array is uniform. The repeated measurements at position 7 are also consistent with the original measurements. In general, the measured cross-polarization beams do not exhibit the deep null on-axis that is seen in the simulations as a result of reflections and misalignments in the NIST VNA system. Reflections in the VNA system are maximized when the receiver and transmitter are head-on, which can result in artifacts in the main lobes of the beams. To account for this in calculations, the beam within the Lyot stop is modeled by a Gaussian summed with an exponential. To calculate the beam coupling efficiency, the measured beams are extrapolated from $\theta \sim 90°$ to $\theta = 180°$ by fitting an exponential decay to the last 15° of the beam measurements. The average measured beam coupling efficiency is in agreement with the simulations at each frequency as can be seen in Figure 14. Small variations as a function of frequency are ascribed to measurement error. The band-averaged beam coupling efficiency of the low band (130-180 GHz) is 68% for the measured beams and 66% for the simulated beams. For the high band (200-270 GHz), the band-averaged beam coupling efficiency is 75% for both the measured and simulated beams.

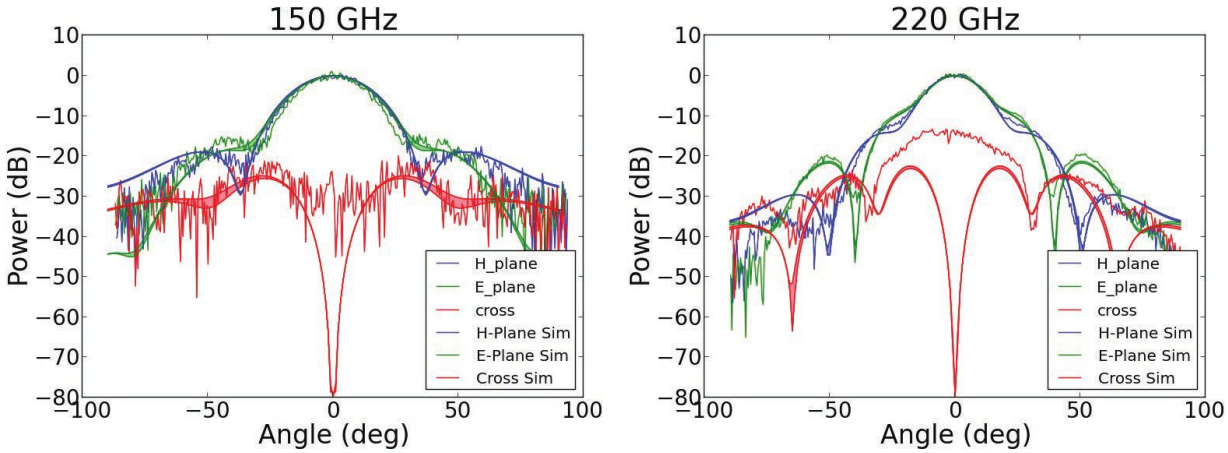

(a) 150 GHz (b) 220 GHz

Figure 12: Measurements of the H-plane (blue), E-plane (green), and cross-polarization (red) beams at a single position are shown above with their theoretical simulations from HFSS. The simulations are the smooth curves. The thickness of the theoretical simulations indicates the difference between simulations with and without a 2° DRIE taper (see § 4.2). The measurements are consistent with the simulations. Note that the VNA system is more susceptible to systematic effects at higher frequencies.

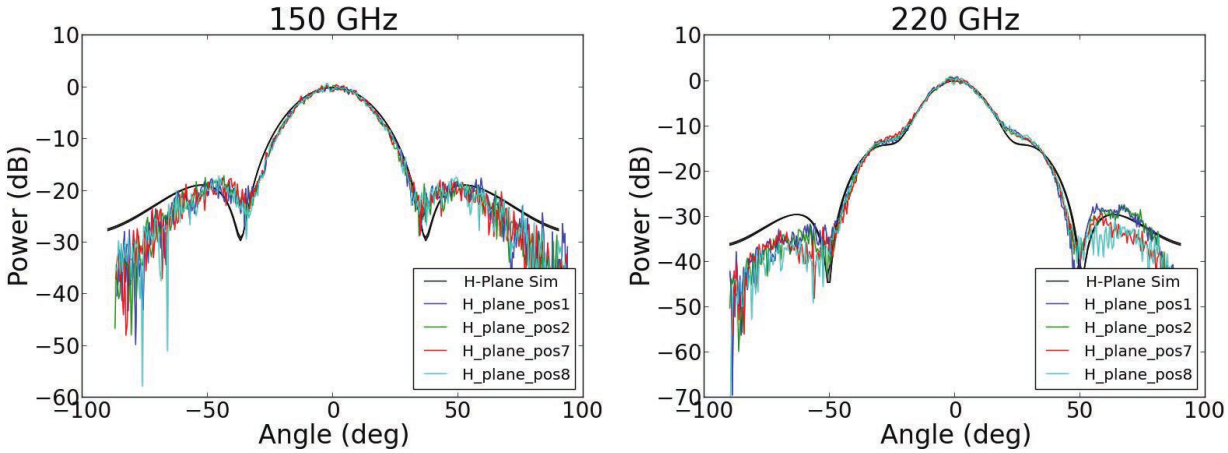

(a) 150 GHz (b) 220 GHz

Figure 13: Measurements of H-plane beams at 150 GHz at each of the four feedhorn positions are shown above. The measurements between horns show that the feedhorns are highly uniform across the array.

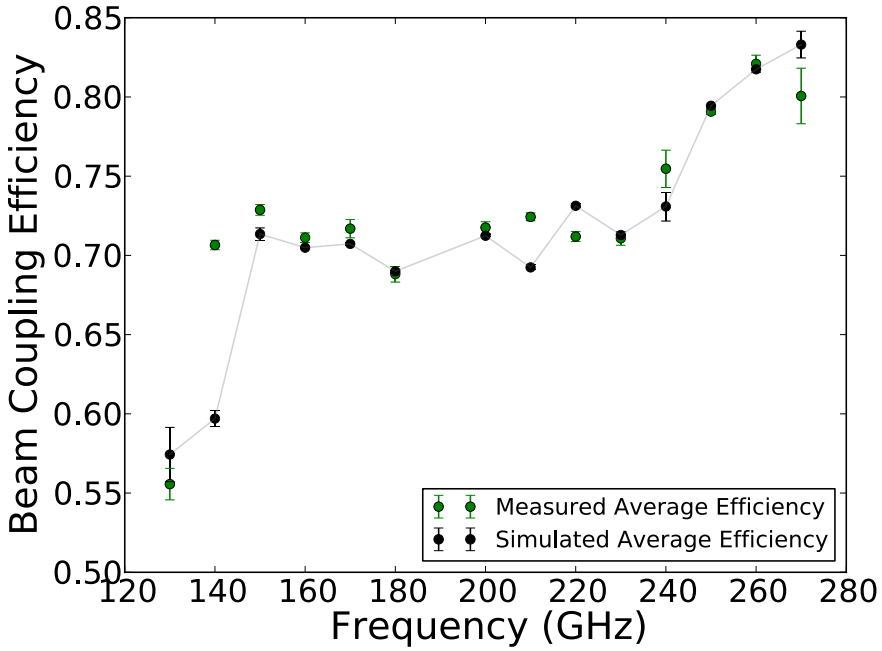

Figure 14: The average beam coupling efficiencies of the measured (green) and simulated (black with grey line) 150/230 GHz feedhorns are shown above as a function of frequency. The simulations and measurements were both performed every 10 GHz. The error bars on the simulations represent the variation between simulations with and without the DRIE taper, and the error bars on the measurements only represent the variance amongst the measurements of the feedhorns at the four positions on the array and do not include systematic contributions. All the efficiencies are consistent within 3.5% except for the value at 140 GHz where the simulated beam coupling efficiency is varying rapidly.

5.1 Future Work

The spline-profiled feedhorns developed for AdvACT are compact and have been shown to have good performance in both beam symmetry and efficiency. The 150/230 GHz feedhorn array has been fabricated, measured, and integrated with the detector array for deployment this summer (2016). NIST has fabricated single pixel test horns for the 90/150 GHz feedhorns, and initial measurements of these horns show that they are in good agreement with the simulations. Fabrication of the full 90/150 GHz feedhorn arrays is currently underway. The 28/41 GHz feedhorn is still in development, but several possible horn candidates have been identified. The use of spline-profiled feedhorns will increase AdvACT's mapping speed by increasing the number of detectors that can fit on each array while maintaining high beam coupling efficiency.

ACKNOWLEDGMENTS

This work is supported by a NASA Office of the Chief Technologist's Space Technology Research Fellowship and NASA Grant NNX13AE56G. AdvACT is supported by the U.S. National Science Foundation through award 1440226. The development of multichroic detectors and lenses was supported by NASA grants NNX13AE56G and NNX14AB58G. The work of KPC, BJK, BLS, and JTW was also supported by NASA Space Technology Research Fellowship awards. We would also like to acknowledge Lindsey Bleem whose feedhorn design for the South Pole Telescope was a helpful guide for this work.

REFERENCES

[1] Seljak, U. b. u. and Zaldarriaga, M., "Signature of gravity waves in the polarization of the microwave background," *Phys. Rev. Lett.* **78**, 2054–2057 (Mar 1997).

[2] Kamionkowski, M., Kosowsky, A., and Stebbins, A., "A probe of primordial gravity waves and vorticity," *Phys. Rev. Lett.* **78**, 2058–2061 (Mar 1997).

[3] Abazajian, K. N., Arnold, K., Austermann, J., Benson, B. A., Bischoff, C., Bock, J., Bond, J. R., Borrill, J., Buder, I., Burke, D. L., Calabrese, E., Carlstrom, J. E., Carvalho, C. S., Chang, C. L., Chiang, H. C., Church, S., Cooray, A., Crawford, T. M., Crill, B. P., Dawson, K. S., Das, S., Devlin, M. J., Dobbs, M., Dodelson, S., Doré, O., Dunkley, J., Feng, J. L., Fraisse, A., Gallicchio, J., Giddings, S. B., Green, D., Halverson, N. W., Hanany, S., Hanson, D., Hildebrandt, S. R., Hincks, A., Hlozek, R., Holder, G., Holzapfel, W. L., Honscheid, K., Horowitz, G., Hu, W., Hubmayr, J., Irwin, K., Jackson, M., Jones, W. C., Kallosh, R., Kamionkowski, M., Keating, B., Keisler, R., Kinney, W., Knox, L., Komatsu, E., Kovac, J., Kuo, C.-L., Kusaka, A., Lawrence, C., Lee, A. T., Leitch, E., Linde, A., Linder, E., Lubin, P., Maldacena, J., Martinec, E., McMahon, J., Miller, A., Mukhanov, V., Newburgh, L., Niemack, M. D., Nguyen, H., Nguyen, H. T., Page, L., Pryke, C., Reichardt, C. L., Ruhl, J. E., Sehgal, N., Seljak, U., Senatore, L., Sievers, J., Silverstein, E., Slosar, A., Smith, K. M., Spergel, D., Staggs, S. T., Stark, A., Stompor, R., Vieregg, A. G., Wang, G., Watson, S., Wollack, E. J., Wu, W. L. K., Yoon, K. W., Zahn, O., and Zaldarriaga, M., "Inflation physics from the cosmic microwave background and large scale structure," *Astroparticle Physics* **63**, 55–65 (Mar. 2015).

[4] Thornton, R. J., Ade, P. A. R., Aiola, S., Angile, F. E., Amiri, M., Beall, J. A., Becker, D. T., Cho, H., Choi, S. K., Corlies, P., Coughlin, K. P., Datta, R., Devlin, M. J., Dicker, S. R., Dunner, R., Fowler, J. W., Fox, A. E., Gallardo, P. A., Gao, J., Grace, E., Halpern, M., Hasselfield, M., Henderson, S. W., Hilton, G. C., Hincks, A. D., Ho, S. P., Hubmayr, J., Irwin, K. D., Klein, J., Koopman, B., Li, D., Louis, T., Lungu, M., Maurin, L., McMahon, J., Munson, C. D., Naess, S., Nati, F., Newburgh, L., Nibarger, J., Niemack, M. D., Niraula, P., Nolta, M. R., Page, L. A., Pappas, C. G., Schillaci, A., Schmitt, B. L., Sehgal, N., Sievers, J. L., Simon, S. M., Staggs, S. T., Tucker, C., Uehara, M., van Lanen, J., Ward, J. T., and Wollack, E. J., "The Atacama Cosmology Telescope: The polarization-sensitive ACTPol instrument," *ArXiv e-prints* (May 2016).

[5] Fowler, J. W., Niemack, M. D., Dicker, S. R., Aboobaker, A. M., Ade, P. A. R., Battistelli, E. S., Devlin, M. J., Fisher, R. P., Halpern, M., Hargrave, P. C., Hincks, A. D., Kaul, M., Klein, J., Lau, J. M., Limon, M., Marriage, T. A., Mauskopf, P. D., Page, L., Staggs, S. T., Swetz, D. S., Switzer, E. R., Thornton, R. J., and Tucker, C. E., "Optical design of the Atacama Cosmology Telescope and the Millimeter Bolometric Array Camera," *Applied Optics* **46**, 3444–3454 (June 2007).

[6] Henderson, S. W., Allison, R., Austermann, J., Baildon, T., Battaglia, N., Beall, J. A., Becker, D., De Bernardis, F., Bond, J. R., Calabrese, E., Choi, S. K., Coughlin, K. P., Crowley, K. T., Datta, R., Devlin, M. J., Duff, S. M., Dunkley, J., Dünner, R., van Engelen, A., Gallardo, P. A., Grace, E., Hasselfield, M., Hills, F., Hilton, G. C., Hincks, A. D., Hložek, R., Ho, S. P., Hubmayr, J., Huffenberger, K., Hughes, J. P., Irwin, K. D., Koopman, B. J., Kosowsky, A. B., Li, D., McMahon, J., Munson, C., Nati, F., Newburgh, L., Niemack, M. D., Niraula, P., Page, L. A., Pappas, C. G., Salatino, M., Schillaci, A., Schmitt, B. L., Sehgal, N., Sherwin, B. D., Sievers, J. L., Simon, S. M., Spergel, D. N., Staggs, S. T., Stevens, J. R., Thornton, R., Van Lanen, J., Vavagiakis, E. M., Ward, J. T., and Wollack, E. J., "Advanced ACTPol Cryogenic Detector Arrays and Readout," *Journal of Low Temperature Physics* (Mar. 2016).

[7] Clarricoats, P. J. B. and Olver, A. D., [*Corrugated horns for microwave antennas*], Peter Peregrinus Ltd., London, UK (1984).

[8] Datta, R., Hubmayr, J., Munson, C., Austermann, J., Beall, J., Becker, D., Cho, H. M., Halverson, N., Hilton, G., Irwin, K., Li, D., McMahon, J., Newburgh, L., Nibarger, J., Niemack, M., Schmitt, B., Smith, H., Staggs, S., Van Lanen, J., and Wollack, E., "Horn Coupled Multichroic Polarimeters for the Atacama Cosmology Telescope Polarization Experiment," *Journal of Low Temperature Physics* **176**, 670–676 (Sept. 2014).

[9] Granet, C., James, G. L., Bolton, R., and Moorey, G., "A smooth-walled spline-profile horn as an alternative to the corrugated horn for wide band millimeter-wave applications," *IEEE Transactions on Antennas and Propagation* **52**, 848–854 (March 2004).

[10] Zeng, L., Bennett, C. L., Chuss, D. T., and Wollack, E. J., "A Low Cross-Polarization Smooth-Walled Horn With Improved Bandwidth," *IEEE Transactions on Antennas and Propagation* **58**, 1383–1387 (Apr. 2010).

[11] Wollack, E. J., U-yen, K., and Chuss, D. T., "Photonic choke-joints for dual-polarization waveguides," 177–180 (May 2010).

[12] Nibarger, J. P., Beall, J. A., Becker, D., Britton, J., Cho, H.-M., Fox, A., Hilton, G. C., Hubmayr, J., Li, D., McMahon, J., Niemack, M. D., Irwin, K. D., Lanen, J., and Yoon, K. W., "An 84 Pixel All-Silicon Corrugated Feedhorn for CMB Measurements," *Journal of Low Temperature Physics* **167**, 522–527 (May 2012).

[13] White, M. and Srednicki, M., "Window functions of cosmic microwave background experiments," *The Astrophysical Journal* **443**, 6–10 (Apr. 1995).

[14] Zaldarriaga, M. and Seljak, U. c. v., "Gravitational lensing effect on cosmic microwave background polarization," *Phys. Rev. D* **58**, 023003 (Jun 1998).

[15] Shimon, M., Keating, B., Ponthieu, N., and Hivon, E., "CMB polarization systematics due to beam asymmetry: Impact on inflationary science," *Physical Review D* **77**, 083003 (Apr. 2008).